European Rotorcraft Forum

SIMULATION AND TESTING OF HELICOPTER-SHIP AERODYNAMIC INTERACTION

N. Taymourtash*, A. Zanotti, G. Gibertini, G. Quaranta
Department of Aerospace Science and Technology - Politecnico di Milano
Campus Bovisa, Via La Masa 34, 20156 Milano, Italy
* Politecnico di Milano and University of Glasgow, e–mail: neda.taymourtash@polimi.it

Abstract
Development of a high-fidelity simulation environment, suitable for Helicopter-Ship Dynamic Interface testing has shown numerous advantages with respect to at-sea test campaigns. To correctly replicate the workload of the pilot, it is crucial to model the unsteady loads caused by complex aerodynamic interaction between airwake of the ship and inflow of the rotor. This paper aims to investigate the behaviour of the unsteady aerodynamic loads on a scaled-helicopter operating in the airwake of a generic frigate model. A series of wind tunnel tests have been conducted to characterise the unsteady loading for a wide range of wind speeds, directions and positions of the helicopter over the deck. A stern landing trajectory was simulated by trimming the rotor at different positions along an oblique path towards the landing spot. The unsteady measurements have been used to evaluate a numerical model developed by integrating the time-accurate CFD airwake of the isolated ship into the simulation environment. The numerical and experimental results show similar behaviour, as moving towards the landing spot the unsteadiness is increased. However, the numerical model underestimates the unsteadiness in most of the test points and the difference becomes more significant when testing with a 60° wind-angle. Furthermore, a fully dynamic landing maneuver was tested in the wind tunnel to evaluate the effect of the approach velocity of the helicopter on the unsteady loads. In comparison to the measurements at fixed positions, the effect of approach velocity was found to be more significant when testing with the wind from the port side compare to the headwind condition.

Keywords: Unsteady Aerodynamic, Wind Tunnel, Ship Landing, Dynamic Interface.

1. INTRODUCTION

Rotorcraft shipboard operations are often characterized by an increased workload for the pilots due to the aerodynamic interaction of the helicopter wake with the flow perturbations caused by the superstructure of the ship. To enhance the safety of such demanding tasks, a series of flight tests are performed to identify the Ship-Helicopter Operational Limitation (SHOL) which defines the boundaries of safe operation for a particular ship-helicopter combination in terms of maximum allowable wind speed and direction relative to the ship [1].

To reduce the number of at-sea trials and improve the pilot training, development of Dynamic Interface Simulation is a promising solution that could be further used to expand the SHOL envelopes and improve the design of future platforms [2,3].

For the purpose of SHOL testing, high levels of fidelity are required for DI simulation which is decomposed into the models and subsystems and further decomposed into the individual elements. Then, the overall fidelity is measured from a quantitative description of fidelity for each constituent element [4,5]. In this regard, airwake modeling is recognized as a crucial element which strongly impacts the overall fidelity. With the majority of the airwake energy concentrated in the bandwidth of 0.2-2 Hz [6], the unsteadiness of the flow field directly affects the handling qualities and pilot closed-loop response which is characterized by a cross-over frequency lower than 1.6 Hz [7]. Also, it has been demonstrated that the correct representation of the time-accurate disturbances are important in replicating the workload experienced by the pilots [8,9].

One of the main challenges involved in the airwake modeling is the interaction of the ship airwake with rotor inflow or other aerodynamic sur-

faces of the helicopter. Although the most representative approach is development of a fully-coupled simulation in which the aerodynamic solver and flight dynamics code should be run simultaneously with the communication between two codes, due to the excessive computational cost, currently this approach cannot support the real-time DI simulations[10,11,12,13]. Another approach to analyse the unsteadiness involved in this mutual interaction is to perform the scaled experiments with the helicopter model operating in the airwake of the ship, while the wind speed and direction can be set according to the SHOL diagram.

Towards this aim, few experimental setups are developed at sub-scale to evaluate the unsteady loading in different phases of the landing maneuver and with respect to various wind conditions. One of the first experimental investigations was done by Zan at Aerodynamic Laboratory, National Research Council of Canada[14]. The initial experiments were conducted with an isolated powered rotor mounted on a sting capable of moving over the deck of a 1:50 scale model of the Canadian Patrol Frigate (CPF). With a fixed incidence setting on the blades, time-averaged thrust was measured on a dynamic balance. This study has demonstrated that the reduced inflow to the rotor, due to the ship airwake, can significantly decrease rotor thrust up to 15%. Following this campaign, another setup was developed aimed at evaluation of the unsteady side-force, yawing moment and drag force applied on a rotor-less Sea King fuselage immersed in the turbulent airwake of CPF[15]. To quantify the unsteady loading, Power Spectral Densities (PSD) were calculated from the time histories of the measured aerodynamic loads and the square-root of the integral over the bandwidth of 0.2 to 2 Hz was taken as the measure of unsteadiness. Across this frequency range, the magnitude of the spectrum represents a portion of the pilot workload associated with response to the airwake turbulence. Consequently, a reasonable correlation was found between RMS loading and pilot workload obtained from flight test. The setup was further modified by adding a 1:50 scale rotor of Sea King to account for the effect of rotor downwash on the fuselage loading[16]. It was shown that in most cases the unsteady loading increased with the presence of the rotor downwash. Also, the level of unsteadiness at different positions over the deck and in different wind speeds was changed compared with the rotor-less case.

Another setup was designed and developed by Wang et al. to measure the unsteady forces and moments imposed by the airwake of a generic ship on a 1:54 scale model of Merlin AW-101 helicopter[17]. The setup, specially designed for testing in a water tunnel, was used to simulate two WOD conditions, including headwind and wind coming with a direction of 45° from the starboard side, conventionally indicated as Green45, and the measurements were conducted at fixed positions along the flight path of a landing maneuver[18]. Time-averaged measurements identified a region of thrust-deficit in headwind and a pressure-wall in the 45° wind angle. The unsteady loading was also compared in terms of severity and showed higher RMS loading in Green45 and particularly through the lateral translation phase. The setup has been used also to investigate the potential benefits of aerodynamic modifications to the ship geometry[19]. Various modifications were proposed and many were found effective in reducing the RMS forces and moments. In particular, the promising design concepts were a side-flap and notch modification which both showed consistent improvements of 25-50% in unsteady loading.

More recently, a setup was developed to study the aerodynamic interaction between a 1:13 scaled-helicopter model and Simple Frigate Shape 1, as a generic ship geometry[20]. Initially, a series of wind tunnel tests were performed to characterise the airwake of the isolated ship in different WOD conditions by means of Particle Image Velocimetry (PIV) technique. Then, the time-averaged aerodynamic loads of the rotor were measured, while the helicopter was placed in a series of points representative of a stern landing trajectory and a vertical descent over the landing spot. Load measurements were performed in two WOD conditions, including headwind and Red30, where red indicates a wind coming from the port side, in addition to a no-wind test. Variation of the mean aerodynamic loads showed a strong ground effect while moving towards the deck. Furthermore, a significant reduction of the pitch moment was identified due to the interaction between the downwash produced by the recirculation zone and the inflow of the rotor.

Towards the development of DI simulation, the focus of this paper is analysis of the unsteady aerodynamic loads of a helicopter model operating inside the airwake of the ship. The setup introduced in[20] has been substantially improved so that a landing trajectory can be simulated while trimming the rotor to obtain a specific set of aerodynamic loads. Taking advantage of this new setup, a series of wind tunnel tests have been conducted in order to investigate the effect of wind speed and direction on the unsteady rotor loads. The new setup was also exploited to simulate a "Dynamic Landing" by setting a constant approach velocity for the helicopter to perform the landing maneuver. Furthermore, to perform the unsteady simulation, a multibody model of the rotor has been developed and coupled with

the time-accurate CFD airwake of the isolated ship based on one-way coupling method. In the following sections, after introducing the experimental setup and test plan, the numerical model and airwake integration will be described. Finally, the experimental and numerical results will be presented and discussed.

2. EXPERIMENTAL SETUP

The experiments were conducted in the large test chamber of the GVPM (Galleria del Vento Politecnico di Milano) with 13.84 m wide, 3.84 m high and length of 35 m. Figure 1 shows the complete setup mounted inside the test chamber. The setup consists of a 4-bladed helicopter and a simplified ship model. The helicopter model was held by a horizontal strut connected to a system of two motorised orthogonal sliding guides which is able to change the relative position of the helicopter in both vertical and longitudinal directions. A fixed reference frame is defined to introduce the test points, representing the position of the rotor hub center with respect to the ship. The XZ plane of the reference frame, as represented in Fig. 2, is aligned with the longitudinal symmetry plane of the deck. All the setup was mounted on the large turning table of the test section with a diameter of 13 m, so that the effect of wind direction could be tested as well.

Figure 1: Test setup mounted inside the test chamber of GVPM.

2.1. Ship Model

The ship model is a 1:12.5 scale model of Simple Frigate Shape 1 which is a highly simplified but representative ship geometry, developed as a part of an international collaboration in which Canada, Australia, New Zealand, UK and USA evaluated the ability of CFD codes to simulate complex airwakes[21].

The SFS1 model consists of a rectangular prism with a step on its rear and another prism on top

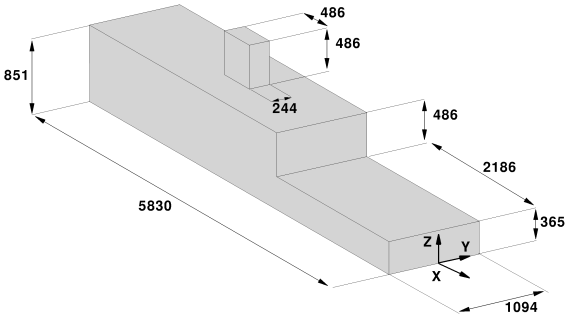

Figure 2: Geometry and dimensions of the 1:12.5-scale model of SFS1.

which is acting as a ship superstructure, as represented in Fig. 2, reporting the main dimensions of the model. The landing point of the helicopter model was placed on the center of the turning table, thus the ship can be rotated to both sides, while the landing point remains fixed with respect to the boundaries of the test section.

The flight deck and hangar wall were equipped with 77 and 35 pressure taps, respectively. The pressure measurements were performed using four low-range 32-ports pressure scanners embedded inside the ship model. The declared accuracy of the pressure scanners led to an estimated uncertainty for the pressure coefficient of approximately 0.15.

A Pitot probe was mounted on top of the superstructure, 180 mm above and 90 mm upstream of the mast, as the reference point for free stream velocity. In each test, the Pitot probe was adjusted in order to have the static port aligned with the wind direction.

2.2. Helicopter Model

The helicopter model consists of a fuselage and a rotor which has four untwisted and untapered rectangular blades, made of carbon-fiber composite materials with NACA0012 airfoil. The rotor, with a diameter of 970 mm, includes a complete swashplate mechanism so that collective and cyclic commands can be applied to the blades to trim the rotor while approaching the flight deck. A polycarbonate fuselage was manufactured with Fused Deposition Modelling (FDM) technique to be representative of a 1:10 scaled-model of Bo105 as a generic medium-size helicopter. The fuselage is mounted on an internal metallic structure housing a six-components strain gauge balance (Koris F6D-80e-60) and the driving motor system for the rotor. A brushless motor, with 3.3 kW continuous power was connected directly to the rotor shaft by means of a joint coupling. The rotor rotational speed was maintained in all tests by

means of an Electronic Speed Controller (ESC) connected to the motor and recorded with the same sampling frequency as the balance loads, so that the load coefficients can be calculated based on the instantaneous RPM of the rotor.

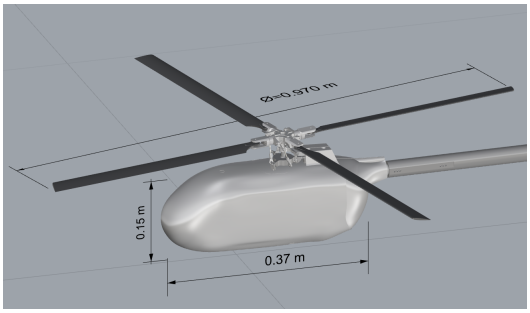

Figure 3: Dimension and layout of the helicopter model.

2.3. Scaling Parameters

The main scaling parameter applied to this investigation is to maintain the Strouhal number of the full-scale model. This matching requires the correct scaling of three parameters, including frequency, geometry, and free stream velocity. Considering Bo-105 as a generic medium size helicopter, the geometric scale, based on rotor radius, is fixed at 1:10.1. The rotational speed of the rotor was selected high enough to increase the Reynolds and Mach numbers, while retaining the wind speed, as required by Strouhal similarity, within the limits of free stream velocity of the test section. Consequently, a frequency scale of 4.75:1 was fixed which leads to the velocity scale of 1:2.1. This velocity scale gives the ship-based Reynolds number in the range of $3.5e5$ to $6.1e5$ while testing in different wind speeds, which satisfies the minimum Reynolds number of 11000 for wind tunnel testing of sharp-edged bodies, like SFS1, to be insensitive to Reynolds number[22]. Some preliminary tests were performed in order to select a thrust level that could be maintained in all test conditions, while avoiding excessive operating temperature and power extraction from the electric motor. Consequently, the resultant thrust coefficient is 60% of the full-scale value. Table 1 presents all parameters of the model compared with Bo-105.

3. TEST PLAN

A typical stern landing trajectory was defined including five points (P1 to P5) along an oblique path with the slope angle of 15° towards the landing point. Furthermore, three additional points (P6 to P8) were

Table 1: Parameters of the experimental model and Bo105.

Characteristic	Scaled Model	Bo105
Number of Blades	4	4
Rotor Radius (m)	0.485	4.91
Angular Speed (rad/s)	211	44.4
Blade Chord (m)	0.042	0.27
Free Stream Velocity (m/s)	4.8-8.4	10.3-18
Advance Ratio	0.047-0.082	0.047-0.082
Tip Mach Number	0.3	0.63
Tip Reynolds Number	$2.9e5$	$3.9e6$
Thrust Coefficient	0.0028	0.0046

Table 2: Coordinate of the test points in ship reference frame.

Test Point	X [mm]	Y [mm]	Z [mm]
P1	1940	0	1450
P2	970	0	1190
P3	0	0	930
P4	-500	0	800
P5	-1000	0	660
P6	-1000	0	930
P7	-1000	0	1060
P8	-1000	0	1190

selected which are representative of a vertical descent over the deck. Figure 4 shows all the test points with the positions listed in Table 2. The coordinates are in the same reference frame introduced in Fig. 2.

To simulate the landing maneuver, the rotor was positioned at each point. Applying collective and cyclic commands, the rotor was trimmed to obtain a specific level of thrust and zero in-plane moments. Then, trim commands were fixed and the acquisition of the loads was performed for 30 seconds with the sampling frequency of 100 Hz and repeated twice for each point.

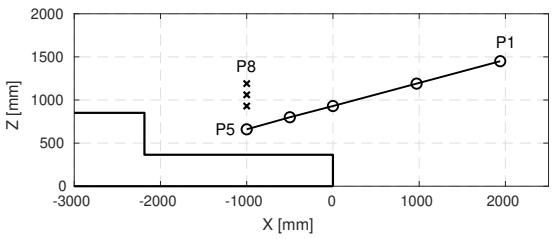

Figure 4: Side-view of the test points. Circles and crosses represent the position of the rotor center in stern landing and vertical descent, respectively.

As required by SHOL analysis, the test conditions were selected based on different wind speeds and directions. Five wind conditions were tested, including two velocities in Head Wind (HW), two velocities in Red Wind from 30° (R30) and one velocity in Red

Wind from $60°$ (R60). Figure 5 shows the selected test conditions in full-scale values.

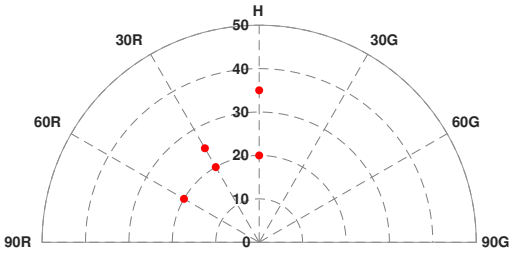

Figure 5: Test points (red dots) imposed on a typical SHOL diagram in full-scale (velocities in knot).

A second approach, called "Dynamic Landing" was tested for three wind conditions. In this approach, helicopter is moving towards the landing point with a constant velocity, while the trim controls, obtained during the static tests for each point, are applied to the rotor. The predefined trajectory, starts with 5 seconds initial hover at P2, after descending towards P5 with a constant velocity of $0.1m/s$, it ends with 5 seconds hover at P5. Regarding the scaling parameters of the test, the selected approach velocity corresponds to a velocity of $1m/s$ with respect to the ship deck in full scale, which is well representative of the final phase of a landing maneuver that is a low speed forward flight near the deck. Figure 6 shows the time history of the longitudinal and vertical position of the rotor during 30 seconds of dynamic maneuver.

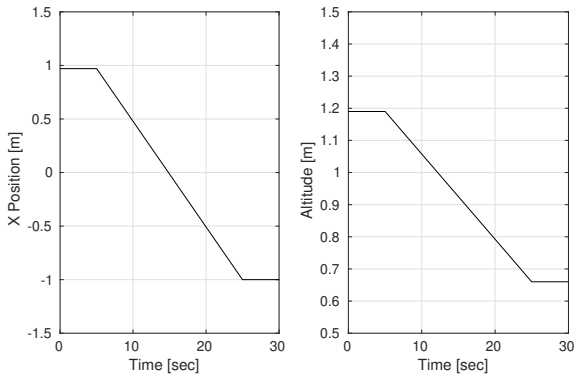

Figure 6: Time history of the longitudinal and vertical position of the rotor in dynamic landing test.

4. NUMERICAL MODEL

A multi-body model of the experimental rotor has been developed using MBDyn, a free general-purpose multi-body dynamics analysis software developed at Politecnico di Milano [23]. MBDyn features the integrated multidisciplinary simulation of multibody systems, including nonlinear mechanics of rigid and flexible bodies subjected to kinematic constraints, along with smart materials, electric and hydraulic networks, active control and essential elements of rotorcraft aerodynamics [24].

The multibody model developed for this study consists of a hingeless, stiff-in-plane rotor with four elastic blades connected to the hub through a revolute hinge, which allows the rotation about the feathering axis of the blade. This degree of freedom, along with a rigid pitch link connected to the swashplate, allows pitch control.

Each blade is modeled by three finite volume beam elements composed of three nodes [25], so that constitutive properties of each section can be defined separately. To introduce the aerodynamic model, *Aerodynamic Beam* element is implemented which relies on the structural beam element to compute the configuration of the aerodynamic surface at each integration point. Aerodynamic loads are computed based on Blade Element/Momentum Theory, using c81 aerodynamic table of NACA0012 defined as the airfoil of the blades. The inflow of the rotor is represented by Pitt-Peters dynamic inflow model [26] with three states, including uniform and linear perturbations of the wake-induced downwash at the rotor disk.

4.1. Ship-Airwake Integration

In order to integrate the airwake of the ship into the numerical model of the rotor, one-way coupling approach is implemented. In this approach, the airwake of the isolated ship is pre-calculated using a steady or unsteady CFD simulation and will be incorporated into the flight dynamics code via look-up tables.

Here, the results of time-accurate CFD simulations performed for the full-scale SFS2 geometry are implemented in the multibody simulation, providing a three-dimensional time-varying velocity field over a region of interest around the deck. The time-varying airwake velocities were stored at every 0.05 seconds for a total time of 30 seconds of time history. Since the flow field can be considered independent with respect to the Reynolds number, the simulations were performed with an inlet velocity of 40 knot and can be scaled for other speeds. Details of the computational approach and validation method can be found in [27]. It should be mentioned that to implement the database in the multibody simulation, the size of the domain and the airwake velocities are scaled using the geometry and velocity scales of the test, introduced in Section 2.3.

To apply the effect of airwake velocity on the aero-

dynamic elements of the rotor, a 3-dimensional interpolation is performed at every time step and for each aerodynamic integration point. So, depending on the position, each aerodynamic element will experience a different local velocity interpolated within the airwake database. Figure 7 shows the contours of time-averaged normalized velocity at the rotor height while placed in the last point of the landing trajectory (P5), with the wind blowing from three different directions, including HW, R30 and R60.

It is clear that in all wind conditions, the fore part of the rotor is inside the recirculation zone, generated immediately behind the hangar wall. However, in headwind condition, a lateral symmetry can be observed which is completely lost when the wind is blowing from the port side.

In order to run the simulation with the unsteady airwake applied to the rotor, a feedback controller is designed in the Simulink environment[28] which is communicating simultaneously with the multibody model, changing the collective and cyclic pitch controls in order to obtain the desired aerodynamic loads, same as the experimental rotor.

5. RESULTS AND DISCUSSION

Here, first the time-averaged loads obtained in the experiment are shown and then the unsteady loading will be presented and compared with the results from the numerical simulations. Finally, the results of the dynamic test, in terms of unsteadiness, will be presented and compared with the measurements at fixed positions.

5.1. Trim Results

As explained in the Section 3, the rotor was trimmed in all points of the landing trajectory to obtain a thrust coefficient of 0.0028 and zero in-plane moments, which could be achieved by applying collective and cyclic controls through the swashplate. Figure 8 compares the average thrust coefficient over 30 seconds of acquisition and two repetitions for each point. Having an average of 0.0028 between all test points and a coefficient of variability of 5%, defined as the ratio of the standard deviation to the mean value, confirms that the desired thrust was achieved within an acceptable tolerance. The coefficients of roll and pitch moments are compared in Fig.9(a) and 9(b), respectively. It should be noted that the objective of the trimming procedure was to set to zero the aerodynamic moments of the rotor. Practically, it was considered acceptable to bring the moments within the range $\pm 0.7 N/m$, to efficiently use the wind tunnel time and avoid over-running the electric motor. As shown in Fig.9, these limits, which corresponds to a moment coefficient of $\pm 1.55 \times 10^{-4}$, are fairly respected in all test points.

5.2. Unsteady Load Analysis

To quantify the unsteady aerodynamic loading of the rotor, the method proposed by Lee and Zan[15,16] is implemented. In this approach, first the PSD is calculated from the measured time-histories of the loads. Then, the square-root of the integral in the bandwidth of interest is considered as a measure of unsteadiness, so-called "RMS loading". As explained in the introduction, the low-frequency content of the airwake, in the bandwidth of 0.2-2 Hz, directly impacts the workload of the pilot. Therefore, the integral should be calculated over the full-scale bandwidth of 0.2-2 Hz, which needs to be correctly mapped into the frequency scale of the test. Figure 10 shows an example of a PSD calculated in both full and test frequency scale. Regarding the frequency scale of 1:4.75, the bandwidth of interest will map into the range of 0.95-9.5 Hz. Here, all the PSD calculations are performed using non-dimensional load coefficients, so the RMS quantities are non-dimensional as well. To convert the recorded time-histories to the frequency domain, Welch's algorithm, also called periodogram method, has been implemented. Welch's method computes an estimate of the power spectral density by dividing the data into overlapping segments, computing a modified periodogram for each segment and averaging the periodograms[29]. The windowing of each individual segment results in reducing the noise in the spectral density estimate, at the expense of frequency resolution.

Power Spectral Density of the thrust coefficient calculated from the time-history of the measured loads and those obtained from the simulation are compared in Figures 11, 12 and 13, referring to headwind, Red30 and Red60, respectively. It should be mentioned that since the first two points of the trajectory (P1 and P2) were outside of the domain of CFD solution, the simulation at these points results in a steady response in terms of rotor loads. This is the reason why these two points are excluded from the unsteady analysis.

Figure 11 shows that in all test points, the simulation can capture the same trend as the experiment with a relatively constant power up to 2 Hz and then decreasing towards the higher frequencies, up to 10 Hz. However, clearly in all points, the spectrum obtained from the simulation is below the one of the test, meaning that the unsteadiness has been underestimated by the simulation. The same be-

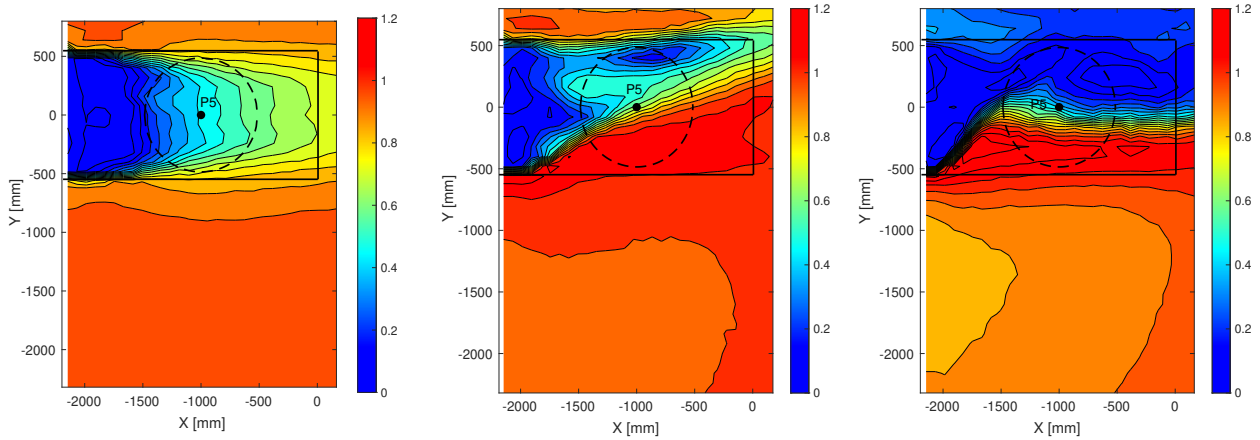

(a) HW (b) R30 (c) R60

Figure 7: Contours of time-averaged non-dimensional airwake velocity ($|\bar{U}|/U_\infty$) at height of P5.

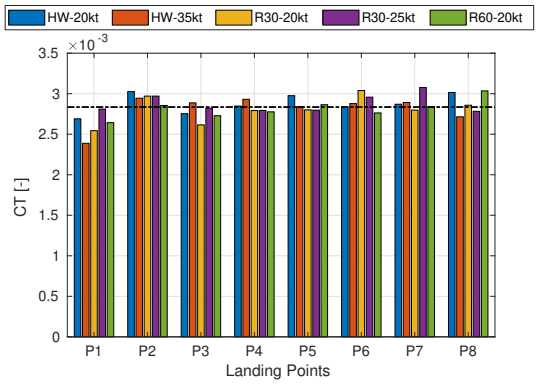

Figure 8: Comparison of time-averaged thrust coefficient for all test points.

haviour can be observed in Red30, however, for the last three points (P6, P7, and P8), the low-frequency part of the spectrum obtained from the simulation has higher energy with respect to the experiment.

Figure 13 compares the PSDs in Red60 test condition. It is clear that in all test points, the simulation is underestimating the unsteadiness and the difference is more significant along the vertical trajectory. Overall, it can be seen that the one-way coupling approach shows a better agreement with the experiment in headwind compared to the tests at non-zero wind angles.

As mentioned before, to quantify the unsteadiness of the aerodynamic loads, the "RMS loading" can be computed from the above PSDs, defined as the following equation:

$$\sigma_x = \sqrt{\int_{f1}^{f2} \bar{S}_{xx}(f)df}$$

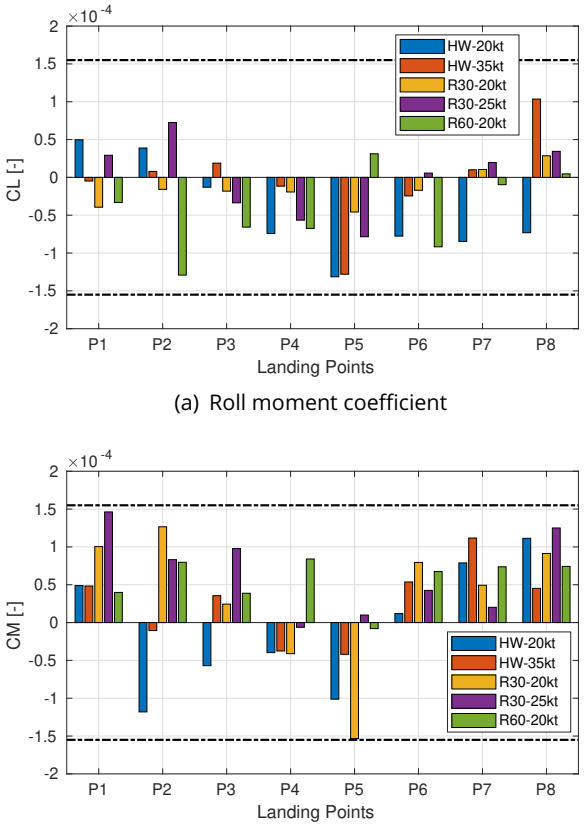

(a) Roll moment coefficient

(b) Pitch moment coefficient

Figure 9: Comparison of moment coefficients for all test points.

This parameter has been calculated for all test points and the results are compared in the following bar charts. It should be mentioned that the experimental value is the average of two repetitions performed at each point.

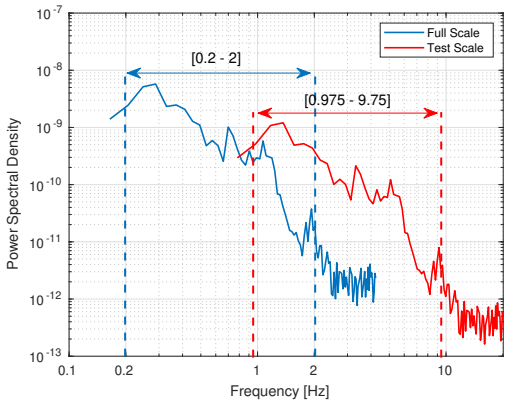

Figure 10: Illustration of the RMS loading calculation in full and test frequency scaling.

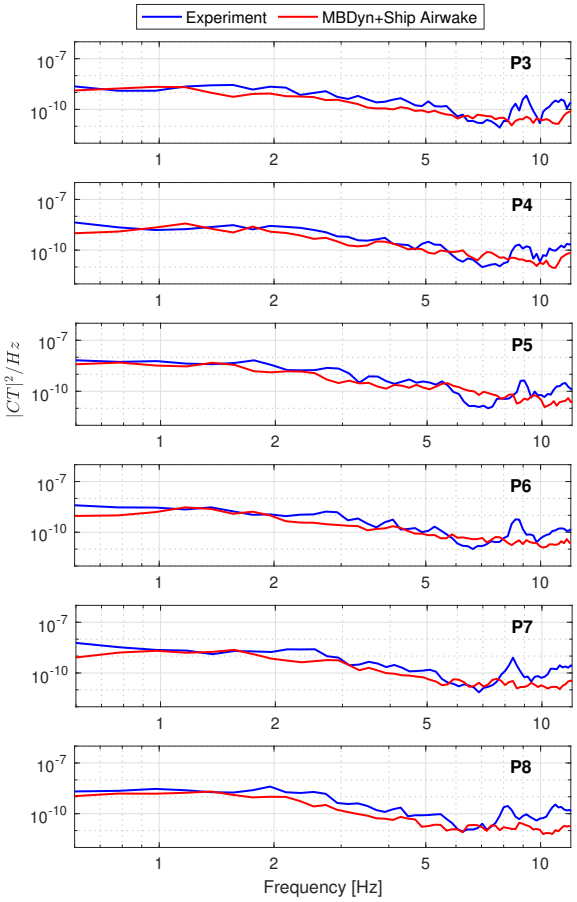

Figure 11: PSD of thrust coefficient derived from measurements and simulation in HW-20kt.

As represented in Fig.14, the numerical simulation follows the trend of the experimental data, as it has the maximum unsteadiness at the landing spot (P5). However, an average error of 25% exists within the eight test points. The same comparison

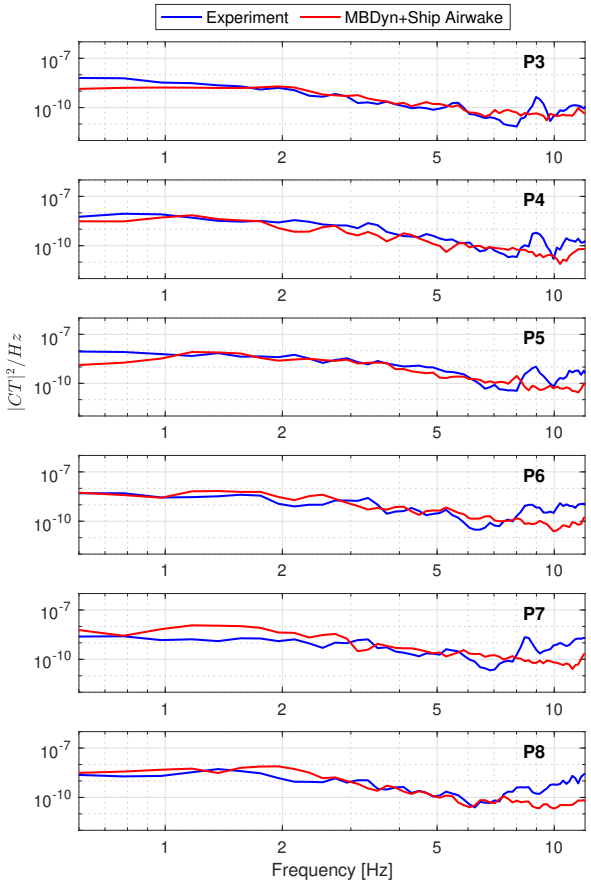

Figure 12: PSD of thrust coefficient derived from measurements and simulation in R30-20kt.

is shown in Fig. 15 for R30 wind condition. As expected from PSDs, the simulation in the last 3 points shows higher unsteadiness compare to the experiment. Here, it can be seen that the error is notable for the last two points, being 60% and 35% higher than the expected values from the test. While the difference remains less than 15% in the first four points.

Figure 16 compares the unsteadiness in Red60 condition in which the rotor experiences a higher lateral wind from the port side compare to the longitudinal component. Clearly, in this condition the simulation is not able to replicate the unsteadiness, however, the desired trim loads were achieved in all test points.

Comparing the last three figures, a similar trend can be observed in all test conditions, in which the unsteadiness is increasing towards the landing point and reaches a maximum value when the rotor is completely immersed in the airwake of the ship. At this point, the unsteady airwake causes severe fluctuations in the aerodynamic response of the rotor. Regarding the low-frequency range of the un-

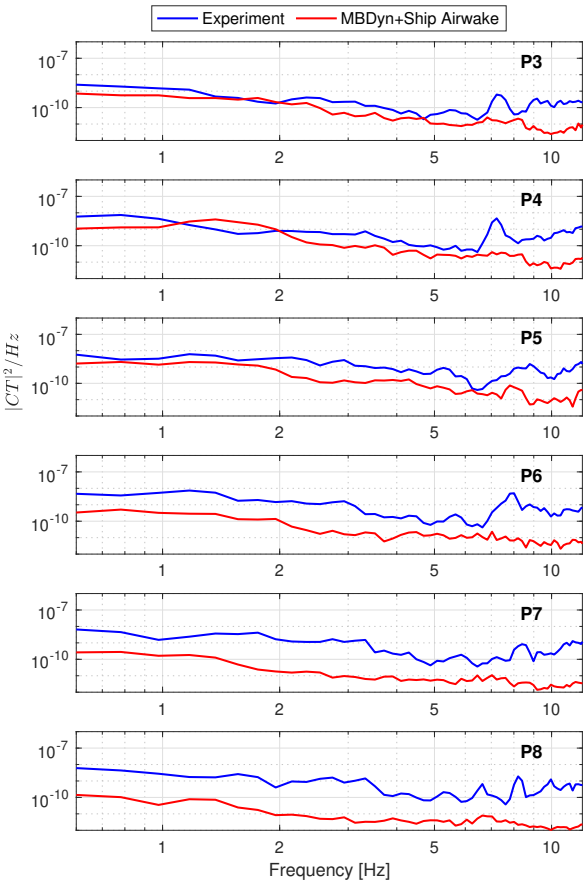

Figure 13: PSD of thrust coefficient derived from measurements and simulation in R60-20kt.

steadiness, it can be concluded that the pilot will experience the highest level of workload while hovering at low-altitude over the landing spot. It is also notable that the Red30 wind condition shows higher unsteadiness with respect to the other wind conditions which is confirmed by both experiment and simulation results.

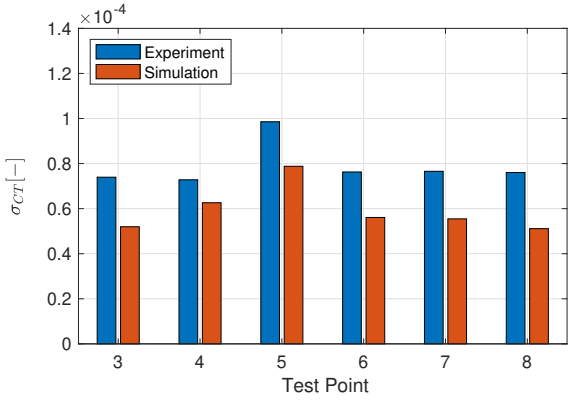

Figure 14: RMS of thrust coefficient derived from measurements and simulation in HW-20kt.

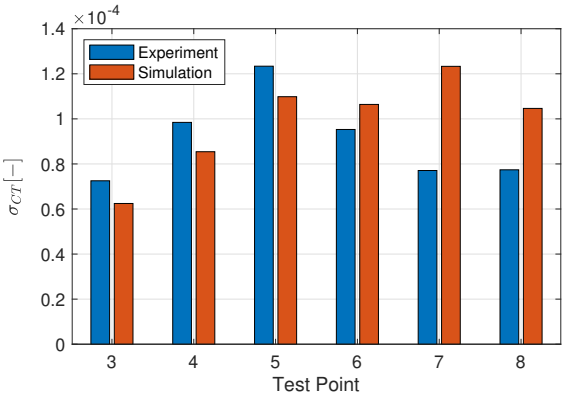

Figure 15: RMS of thrust coefficient derived from measurements and simulation in R30-20kt.

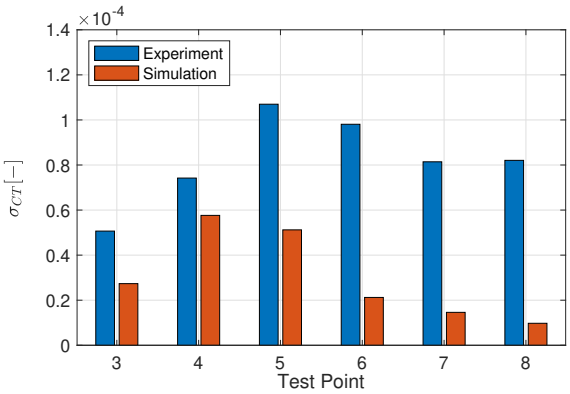

Figure 16: RMS of thrust coefficient derived from measurements and simulation in R60-20kt.

5.3. Dynamic Testing

As mentioned before, dynamic approach consists of 5 seconds initial hover at P2, moving with a constant velocity of $0.1m/s$ towards the landing point, followed by 5 seconds hover at P5. The total acquisition of 30 seconds is used to calculate the PSD of the measured loads, so that the RMS loading can be compared with the previous measurements at each point.

Figure 19 shows the RMS loading of the dynamic approach in comparison with the other 4 points of the trajectory. A weighted average of the unsteadiness obtained at each point has been calculated based on the fractions of total time spent between these four points. To have a better comparison with the dynamic test, this mean value is also presented in the fifth column. It can be seen that in both headwind tests, the weighted average of the unsteady thrust represents a very good correlation with the dynamic approach, as the difference in each test is only 2%. However, in Red30 test condition, the

weighted average is 15% less than the unsteadiness measured in the dynamic approach. This comparison suggests that neglecting the approach velocity and performing the quasi-static simulations may result in underestimation of the unsteady response and workload of the pilot. However, additional tests with different velocities and other directions should be performed to confirm this observation.

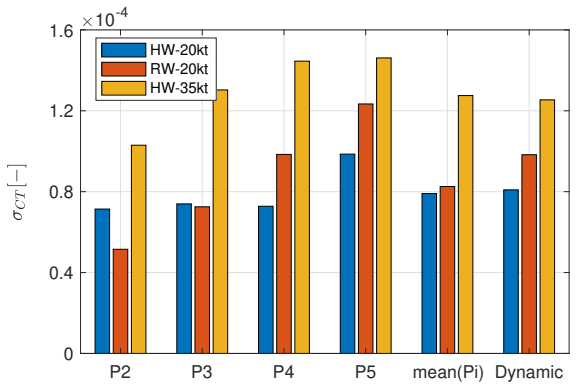

Figure 17: RMS of thrust coefficient derived from static measurements and dynamic approach.

Also, the simulation has been performed with the same approach velocity, so that the unsteady loading obtained from the dynamic approach can be compared with the experiment. As shown in Fig. 18, the overall trend is better captured when testing in lower wind speed (20 knot). While, with the wind speed of 35 knot, it can be seen that the numerical spectrum is reduced in the range of frequencies above 2 Hz. Figure 19 compares the RMS values obtained from the spectrums and shows the difference of 15% in test with the wind speed of 35 knot. Since the initial part of the trajectory is outside the region of interest for the CFD solution, it can be expected to improve the numerical results by enlarging this domain.

6. CONCLUSIONS

A series of wind tunnel tests have been conducted in order to investigate the unsteady aerodynamic loading of a scaled-helicopter in the airwake of a generic frigate model. Time-averaged and unsteady rotor loads were measured for a range of wind speed, direction and positions over the deck. The rotor was placed at a sequence of points, representative of a stern landing trajectory and trimmed for a constant level of thrust and zero in-plane moments by means of collective and cyclic pitch controls applied through the swashplate mechanism implemented in the model.

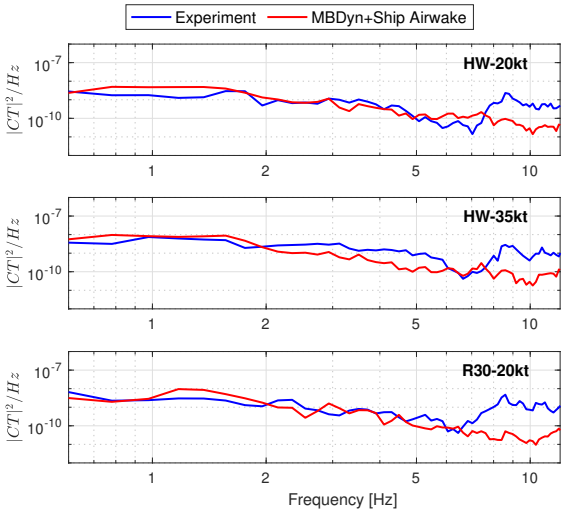

Figure 18: PSD of thrust coefficient in dynamic approach derived from measurement and simulation.

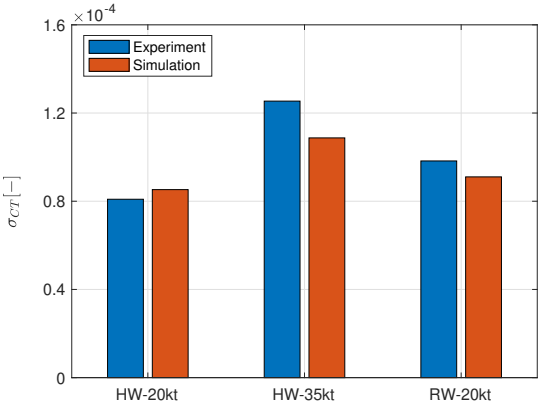

Figure 19: RMS of thrust coefficient in dynamic approach - comparison of simulation and experiment.

Furthermore, a multi-body model of the experimental rotor has been developed to perform the simulation in the same conditions as the wind tunnel tests. To add the effect of ship airwake, a time-accurate CFD database of the velocity field around the deck of the isolated frigate model has been integrated into the simulation based on the one-way coupling method. The unsteady thrust obtained from the coupled simulation was compared with the measurements, over the frequency range of interest.

The experimental results showed that in all test conditions, the unsteadiness is increased by moving towards the landing spot and the highest unsteadiness is experienced by the rotor at the lowest altitude and closest position to the hangar wall. The same trend could be observed in the simulation results, however, the unsteadiness was underesti-

mated in most of the test points. Deficiency of the one-way coupling approach became more evident when testing with the wind from 60°.

Moreover, the effect of approach velocity on the unsteady thrust was examined by performing a dynamic landing maneuver. Comparing the unsteadiness obtained from dynamic tests with the measurements at fixed-positions, confirmed a reasonable correlation in unsteady thrust for the tests in headwind condition. However, in Red30 the static approach results in a lower unsteadiness, if compared with dynamic testing. These results suggest that taking into account the dynamics of the approach could be important while implementing the unsteady loads which are measured or computed using a fully-coupled environment. However, to better quantify the effect of this parameter, additional experiments would be required in other wind conditions, in terms of both wind speed and direction.

ACKNOWLEDGMENTS

This research was supported by NITROS (Network for Innovative Training on ROtorcraft Safety) project which has received funding from the European Union's Horizon 2020 research and innovation program under the Marie Skłodowska-Curie grant agreement No. 721920.

REFERENCES

[1] Hoencamp, A., "An Overview of SHOL Testing Within The Royal Netherlands Navy," 35th European Rotorcraft Forum, 2009.

[2] Owen, I., White, M. D., Padfield, G. D., and Hodge, S. J., "A virtual engineering approach to the ship-helicopter dynamic interface a decade of modelling and simulation research at the University of Liverpool," *The Aeronautical Journal*, Vol. 121, (1198), 2013, pp. 1233–1248.

[3] Roper, D. M., Owen, I., Padfield, G. D., and Hodge, S. J., "Integrating CFD and piloted simulation to quantify ship-helicopter operating limits," *The Aeronautical Journal*, Vol. 110, (1109), 2006, pp. 419–428.
doi: 10.1017/S0001924000001329

[4] Wilkinson, C. H., VanderVliet, G. M., and Roscoe, M. F., "Modeling and Simulation of the Ship-Helicopter Environment," AIAA Modeling and Simulation Technologies Conference and Exhibit, 2001.

[5] Wilkinson, C. H., Roscoe, M. F., and VanderVliet, G. M., "Determing Fidelity Standards for the Shipboard Launch and Recovery Task," AIAA Modeling and Simulation Technologies Conference and Exhibit, 2001.

[6] Hodge, S. J., Zan, S. J., Roper, D. M., Padfield, G. D., and Owen, I., "Time-Accurate Ship Airwake and Unsteady Aerodynamic Loads Modeling for Maritime Helicopter Simulation," *Journal of the American Helicopter Society*, Vol. 54, (2), April 2009, pp. 022005–1–16.

[7] McRuer, D. T., "Interdisciplinary Interactions and Dynamic Systems Integration," *International Journal of Control*, Vol. 59, (1), 1994, pp. 3–12.
doi: 10.1080/00207179408923067

[8] Bunnel, J. W., "AN INTEGRATED TIME-VARYING AIRWAKE IN A UH-60 BLACK HAWK SHIPBOARD LANDING SIMULATION," AIAA Modeling and Simulation Technologies Conference and Exhibit, 2001.

[9] Lee, D., Sezer-Uzol, N., Horn, J. F., and Long, L. N., "Simulation of Helicopter Shipboard Launch and Recovery with Time-Accurate Airwakes," *Journal of Aircraft*, Vol. 42, (2), 2005, pp. 448–461.
doi: 10.2514/1.6786

[10] Crozon, C., Steijl, R., and Barakos, G. N., "Coupled flight dynamics and CFD – demonstration for helicopters in shipborne environment," *The Aeronautical Journal*, Vol. 122, (1247), jan 2018, pp. 42–82.
doi: 10.1017/aer.2017.112

[11] Tan, J. F., Zhou, T. Y., Sun, Y. M., and Barakos, G. N., "Numerical investigation of the aerodynamic interaction between a tiltrotor and a tandem rotor during shipboard operations," *Aerospace Science and Technology*, Vol. 87, 2019, pp. 62–72.
doi: https://doi.org/10.1016/j.ast.2019.02.005

[12] Oruc, I. and Horn, J. F., "Coupled Flight Dynamics and Computational Fluid Dynamics Simulations of Rotorcraft/Terrain Interactions," *Journal of Aircraft*, Vol. 54, (6), June 2017, pp. 2228–2241.
doi: 10.2514/1.C034101

[13] Oruc, I., Horn, J. F., Shipman, J., and Polsky, S., "Towards Real-Time Pilot-in-the-Loop CFD Simulations of Helicopter/Ship Dynamic Interface," *International Journal of Modeling, Simulation, and Scientific Computing*, Vol. 8, (4), 2017.
doi: 10.1142/S179396231743005X

[14] Zan, S. J., "Experimental determination of rotor thrust in a ship airwake," *Journal of the American Helicopter Society*, Vol. 47, (2), 2002, pp. 100–108.
doi: 10.4050/JAHS.47.100

[15] Lee, R. G. and Zan, S. J., "Wind tunnel testing of a helicopter fuselage and rotor in a ship airwake," *Journal of the American Helicopter Society*,

Vol. 49, (2), 2004, pp. 149–159.
doi: 10.4050/1.3092869
[16] Lee, R. G. and Zan, S. J., "Wind tunnel testing of a helicopter fuselage and rotor in a ship airwake," *Journal of the American Helicopter Society*, Vol. 50, (4), 2005, pp. 326–337.
doi: 10.4050/1.3092869
[17] Wang, Y., Curran, J., Padfield, G. D., and Owen, I., "AirDyn: an instrumented model-scale helicopter for measuring unsteady aerodynamic loading in airwakes," *Measurement Science and Technology*, Vol. 22, (4), 2011, pp. 045901.
doi: 10.1088/0957-0233/22/4/045901
[18] Kääriä, C. H., Wang, Y., Padfield, G. D., Forrest, J. S., and Owen, I., "Aerodynamic Loading Characteristics of a Model-Scale Helicopter in a Ship's Airwake," *Journal of Aircraft*, Vol. 49, (5), 2012, pp. 1271–1278.
doi: 10.2514/1.C031535
[19] Kääriä, C. H., Wang, Y., White, M. D., and Owen, I., "An experimental technique for evaluating the aerodynamic impact of ship superstructures on helicopter operations," *Ocean Engineering*, Vol. 115, 2021.
doi: 10.1016/j.oceaneng.2012.12.052
[20] Taymourtash, N., Zagaglia, D., Zanotti, A., Muscarello, V., Gibertini, G., and Quaranta, G., "Experimental study of a helicopter model in shipboard operations," *Aerospace Science and Technology*, Vol. 61, 2013, pp. 97–108.
doi: 10.1016/j.ast.2021.106774
[21] Wilkinson, C., Zan, S. J., Gilbert, N. E., and Funk, J. D., "Modelling and Simulation of Ship Airwakes for Helicopter Operations: A Collaborative Venture," AGARD Symposium on Fluid Dynamics Problems of Vehicles Operating near or in the Air-Sea Interface, 1999.
[22] Healey, J. V., "Establishing a Database for Flight in the Wakes of Superstructures," *Journal of Aircraft*, Vol. 29, (4), 1992, pp. 559–564.
doi: 10.2514/3.46202
[23] Masarati, P., Morandini, M., and Mantegazza, P., "An efficient formulation for general-purpose multibody/multiphysics analysis," *ASME Journal of Computational Nonlinear Dynamics*, Vol. 9, (4), July 2014, pp. 041001–041001–9.
[24] Masarati, P., Piatak, D. J., Quaranta, G., Singleton, J. D., and Shen, J., "Soft Inplane Tiltrotor Aeromechanics Investigation Using Two Comprehensive Multibody Solvers," *Journal of the American Helicopter Society*, Vol. 53, (2), 2008, pp. 179–192.
[25] Ghiringhelli, G. L., Masarati, P., and Mantegazza, P., "Multibody Implementation of Finite Volume C Beams," *AIAA Journal*, Vol. 38, (1), January 2000, pp. 131–138.
[26] Peters, D. A., Boyd, D. D., and He, C. J., "Finite-State Induced-Flow Model for Rotors in Hover and Forward Flight," *Journal of the American Helicopter Society*, Vol. 34, (4), October 1989, pp. 5–17.
[27] Forrest, J. S., J, H. S., Owen, I., and Padfield, G. D., "An investigation of ship airwake phenomena using time-accurate CFD and piloted helicopter flight simulation," 34th European Rotorcraft Forum, Liverpool, UK, September 2008.
[28] *MATLAB R2019b*, The MathWorks Inc., Natick, Massachusetts, 2019.
[29] Welch, P. D., "The Use of Fast Fourier Transform for the Estimation of Power Spectra: A Method Based on Time Averaging Over Short, Modified Periodograms," *IEEE Transactions on Audio and Electroacoustics*, Vol. 15, (2), 1967, pp. 70–73.
doi: 10.1109/TAU.1967.1161901